Development of the Fibrillar and Microfibrillar Structure During Biomimetic Mineralization of Wood

*Gerhard Fritz-Popovski, Daniel Van Opdenbosch, Cordt Zollfrank, Barbara Aichmayer, and Oskar Paris**

Wood is a hierarchical composite, consisting at its lowest hierarchy level of crystalline cellulose elementary fibrils with diameters of 2–4 nm embedded in a matrix of hemicelluloses and lignin. At the micrometer scale, it has a cellular architecture resembling a honeycomb structure. The transformation of the hierarchical wood structure into a silica replica has been reported recently. Its formation process and structural details are studied in this contribution. First, a silica/biopolymer composite is prepared by wood delignification and cell-wall modification, followed by silica precursor infiltration and condensation. The calcination process is monitored to gain insight into the structure development upon decomposition of the biopolymers. The material changes its architecture gradually from fibrillar structures of 10–20 nm in diameter with homogeneous electron density, into fibrils of 8–10 nm in diameter with inhomogeneous electron density, exhibiting internal sub-fibrillar structures of about 2 nm in diameter. The steps of the successful replication of the cellulose elementary fibrils into nanopores of similar diameter and orientation in a fibrillar silica matrix are demonstrated. These nanopore replicas of the original cellulose are wound in a steep helix within the macropore walls. These advanced materials may have lightweight structural applications and the nanopores may be advantageous for molecular separation.

1. Introduction

Biomimetic mineralization is a powerful tool that takes structures formed by a biological process as templates to synthesize inorganic functional materials.[1–3] It offers the advantage to fabricate materials that are difficult to produce by top-down fabrication methods and that have chemical compositions which cannot be produced by self-assembly.[4,5] While the fabrication of nanoparticles, nanowires, and nanotubes by templating of macromolecules (proteins or DNA) or viruses is already quite advanced,[2] the replication of several hierarchical levels in whole biological tissues is still a big challenge. Especially natural multifunctional materials such as plant tissue or arthropod cuticle consist of complex hierarchical structures,[2,5–11] which may be useful for a wide range of potential applications when replicated by inorganic materials.

Wood is a multifunctional material that is structured on several levels of hierarchy. The xylem of soft-woods is dominated by tube-like wood cells (tracheids) with diameters from 10–40 μm and length to diameter ratios of about 100.[12] The cell walls are arranged in several layers, each of them comprising a biopolymer composite material. Several models have been proposed for the spatial arrangement of these biopolymers.[13–16] In the secondary (S2) cell wall layer, which accounts for more than 80% of the cell wall volume,[17] parallel microfibrils are arranged helically around the lumen of the tracheids. These microfibrils have diameters of approximately 10–20 nm,[13] and the angle between the fibril direction and the direction of the tracheid fiber, the microfibril angle MFA, is 3–5° in normal wood, but can be as high as 50° in compression wood.[18] The matrix space between the fibrils is filled with lignin. The microfibrils themselves consist of cellulose elementary fibrils with diameters of 2–4 nm[19] and hemicelluloses, specifically glucomannan between the elementary fibrils and xylan at the surface linking the fibrils to the surrounding lignin.[13] **Figure 1**a shows a simplified sketch of the distribution of the biopolymers at the nanometer level according to the current literature knowledge.[13]

The cellular structure of wood at the micrometer level has been replicated using a variety of substances.[20–27] The replication of the subcellular structure at all hierarchical levels from macroscopic down to the microfibrillar level has so far only rarely been reported.[28–30] Recently, we have succeeded in replicating the structure of wood into silica from the macroscopic down to the microfibrillar level.[31] The nanostructural and structure development details of these hierarchical materials have however not yet been elucidated. In particular, it is not clear whether the structures at the lowest hierarchy

Dr. G. Fritz-Popovski, Prof. O. Paris
Institute of Physics
Montanuniversitaet Leoben
Franz-Josef-Str. 18, 8700 Leoben, Austria
E-mail: oskar.paris@unileoben.ac.at
D. Van Opdenbosch, Prof. C. Zollfrank
Biogene Polymere
Technische Universität München
Schulgasse 16, 94315 Straubing, Germany
Dr. B. Aichmayer
Department of Biomaterials
Max Planck Institute of Colloids and Interfaces
Wissenschaftspark Potsdam-Golm, 14424 Potsdam, Germany

DOI: 10.1002/adfm.201201675

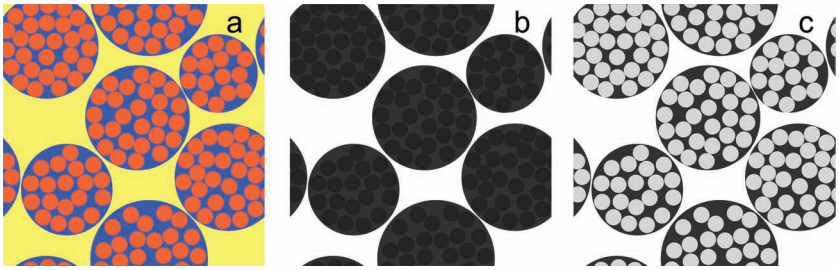

Figure 1. a) Schematic representation of the cross section of wood microfibrils after Fahlén and Salmén.[13] Lignin is represented in yellow, hemicelluloses in blue, and cellulose in orange. The size of the microfibrils is in the order of 10–20 nm and the one of the cellulose elementary fibrils is about 2–3 nm. Inter- and intrafibrillar components are shaded with white for zero and black for a high electron density (b,c). The electron density ratios of 1.07 (b) and 0.20 (c) correspond to those at the beginning and at the end of the calcination process.

level, i.e., the cellulose elementary fibrils, are replicated by the approach. This is crucially dependent on whether the tetraethyl orthosilicate (TEOS) silica precursor molecules can enter the space between the elementary fibrils after lignin removal, i.e., on whether the swellable hemicelluloses can take up a sufficient amount of TEOS to provide a stable silica framework during calcination of the samples. It is known that hemicelluloses and cellulose have a different thermal stability.[32] Therefore, small angle X-ray scattering (SAXS) during the heating (calcination) of different samples provides the possibility to study the nanostructural development in situ. This allows to assess the electron density distribution of the different components during the decomposition of the biopolymers, by using a simple model for the secondary cell wall components (Figure 1b,c).

2. Sample Description

The investigation is based on three sample series, each containing three different samples. Their preparation is described in more detail in the experimental section. Wood thin sections were first extracted with organic solvents leading to a sample called extr. Such samples were consequently delignified resulting in a sample called delig. Functionalization of such samples with maleic acid anhydride lead to samples called MA. Each of these samples could be infiltrated with TEOS resulting in infiltrated samples extr inf, delig inf, and MA inf. By performing a second infiltration cycle, the double infiltrated samples extr 2inf, delig 2inf, and MA 2inf were obtained.

3. Results and Discussion

3.1. Transmission Electron Microscopy

Transmission electron microscopy (TEM) images obtained from the several preparation steps before calcination do not show clear-cut fibrillar structures without additional staining, owing to a too low contrast between the fibrils and their matrix. **Figure 2** shows a representative TEM image of a 2inf sample that was calcined at 500 °C. The image is from the outer part of two adjacent cell walls separated by a bright layer where the lignin-rich middle lamella used to be. Three different layers are recognized corresponding to the original primary (P), secondary 1 (S1) and secondary 2 (S2) cell wall layers. This assignment is not only suggested from the correct spatial extension (P ≈ 100 nm, S1 ≈ 250 nm, S2 > 1.5 μm),[17] but also by the fact that the contrast between the layers is obviously due to different orientations and densities of fibrils within these layers.[12] The regions in the S2 part are dominated by roughly horizontally oriented fibrillar structures, with a slight inclination with respect to the direction of the middle lamella (see inset of Figure 2). One can observe the parallel orientation of the fibrils within the S2 layer, and the change of their orientation in the S1 layer. The distance between neighboring fibrils in the S2 part is estimated to be 12 nm ± 3 nm. Therefore, these structures unequivocally represent the replicated microfibrils of the S2 layer. Although conventional TEM imaging clearly demonstrates the preservation of fibrillar nanostructures in the S2 cell wall layer after calcination of delignified and TEOS infiltrated wood, it cannot resolve easily potential sub-structures within these fibrils. Thus, the question about the potential preservation of the cellulose elementar fibril structural features will be answered by SAXS.

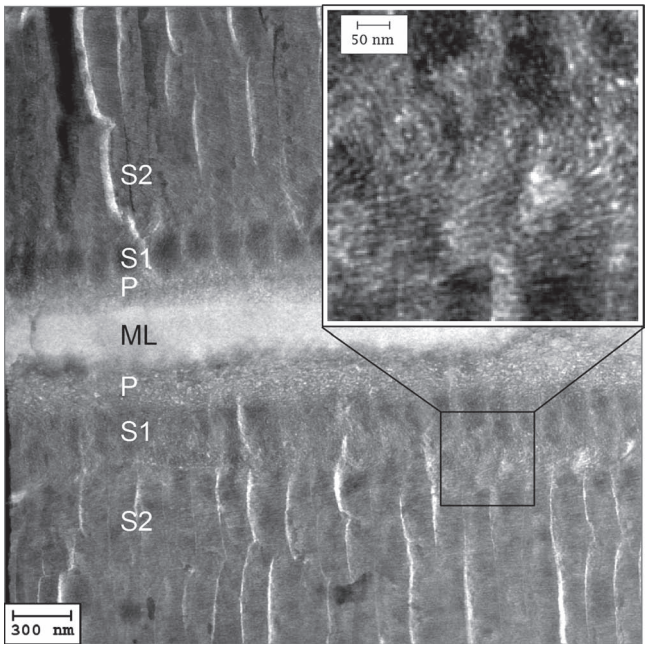

Figure 2. TEM image of the delignified, twice TEOS infiltrated sample after calcination at 500 °C. Cell wall layers, i.e., middle lamella (ML), pimary- (P) and secondary- (S1, S2) layers, are indicated. The eye-catching bright vertical lines are artifacts created by the edge of the cutting tool. The inset has been zoomed and contrast enhanced electronically.

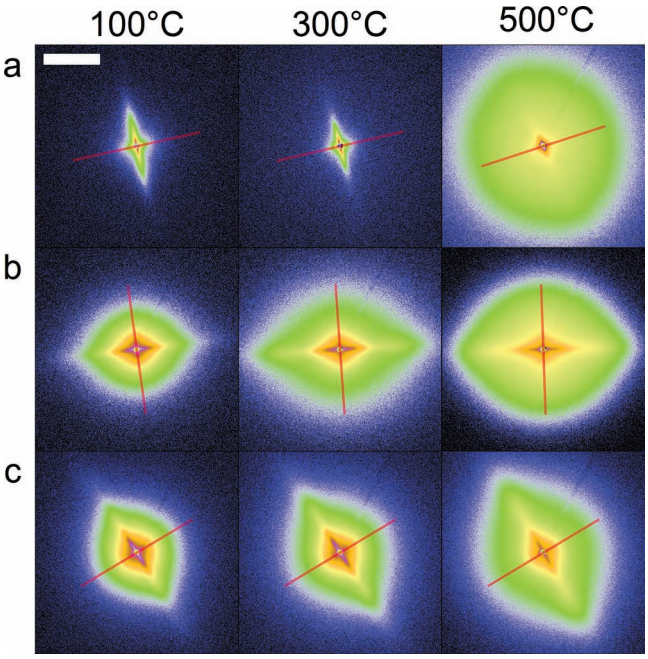

Figure 3. 2D SAXS patterns at different temperatures after infiltration with TEOS: a) solvent extracted wood (sample extr 2inf), b) delignified wood (sample delig 2inf), and c) functionalized wood (sample MA 2inf). The red lines indicate the orientation of the cell axis. The length of the scattering vector is given by the bar (2 nm^{-1}) and the intensity is shown by a logarithmic color-coded scale.

3.2. In Situ Small-Angle Scattering: Qualitative Assessment

2D SAXS on the monolithic samples can provide unique information on the size, arrangement, and orientation of nanometer sized structural units. A first immediate impression on the degree of nanometer structure preservation during in situ calcination is obtained from the anisotropy of the 2D scattering patterns (**Figure 3** and Supporting Information). The characteristic single streak in the 2D scattering patterns is due to the preferred orientation of structures that are oriented with their long axis close to parallel to the cell axis. They can be seen in the scattering patterns from all samples, which means that the orientation of structural features was always at least partly preserved. However, they do not necessarily display preferred orientation of fibrillar structures at nanometer length scales. The surface of the cell walls, as well as drying cracks at the interface between the different cell wall layers may be responsible for such streaks at very low values of the scattering vector q (see Figure 3). Thus, only when the streak clearly extends to large scattering vectors, this can be taken as indicative of the preservation of fibrillar orientation. At temperatures above 290 °C, no such preferred orientation is found in the samples that were not infiltrated (extr, delig, and MA), which suggests the expected total disintegration of the microfibrillar and elementary fibrillar cell wall structure. Similarly, the non-delignified but infiltrated samples extr inf and extr 2inf do not show an anisotropic SAXS signal at large q at elevated temperatures (Figure 3a). By contrast, all delignified and TEOS infiltrated samples (delig inf, delig 2inf, MA inf and MA 2inf) do show a strongly anisotropic

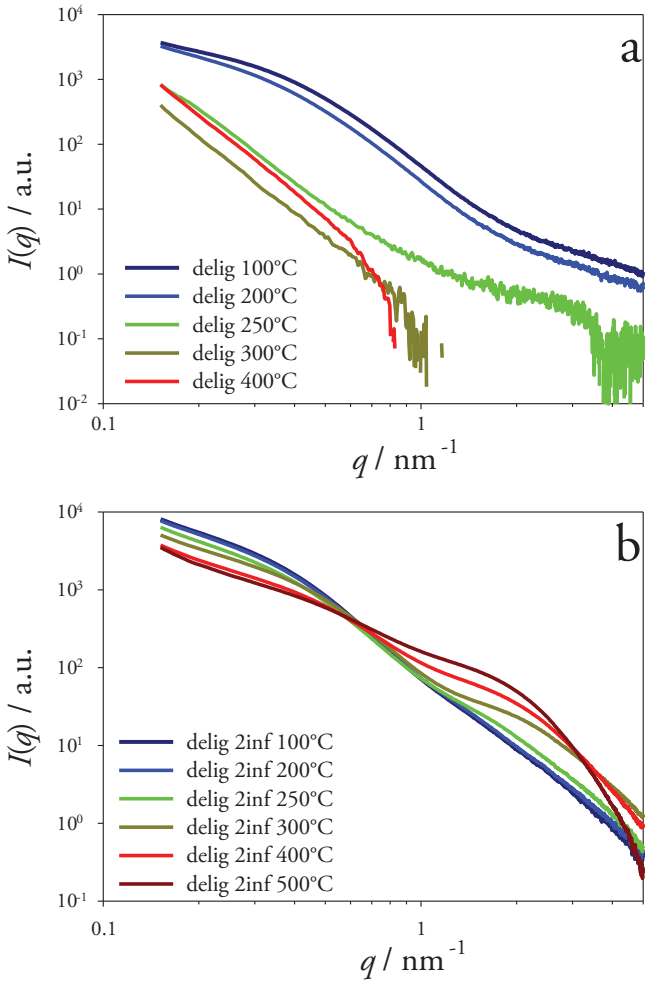

Figure 4. Scattering curves as a function of temperature for the delignified samples: a) without (sample delig) and b) with TEOS infiltration (sample delig 2inf).

SAXS signal with no significant change of the anisotropy with increasing temperature.

The samples can be further analyzed qualitatively on the basis of their power law scattering behavior. A representative example for the 1D scattering function $I(q)$ obtained from the averaging of the 2D patterns (see Experimental Section) is shown in **Figure 4**. At low temperatures, $I(q)$ shows a q^{-1} dependence at low q indicating long cylindrical structures. The shoulder at $q \approx 0.4$ nm^{-1} suggests that the smallest dimension of these structures is in the order of $2\pi/q \approx 15$ nm. For the samples that were not TEOS infiltrated, the intensity strongly decreases with temperature (note the logarithmic intensity scale), indicating the loss of material due to thermal degradation. The $I(q)$ curves show a q^{-4} dependence over the entire q-range at higher temperatures (Figure 4a), which can be explained simply by scattering from surfaces.[33] This suggests that the fibrillar level is already largely destroyed at 250 °C in agreement with the loss of orientation seen in the scattering patterns. Figure 4b shows the scattering curve of the delignified and twice TEOS infiltrated sample. These samples kept the q^{-1} slope at low q and the shoulder at about 0.4 nm^{-1}, but a second shoulder developed

progressively at q-values of about 2 nm^{-1} upon sample heating. This strongly indicates that the fibrillar structures remain intact, and that smaller units become apparent. As these smaller units share the preferred orientation with the fibrillar structures (see the faint streaks in Figure 3b,c), we interpret this by the selective removal of components of the composite fibril material, whose electron densities were originally very similar. The delignified, maleic acid anhydride functionalized and infiltrated samples (MA inf, MA 2inf) showed qualitatively a very similar behavior as the delig samples. The non-delignified samples (extr inf and extr 2inf) show a q^{-4} decay at low q and a shoulder at about 2 nm^{-1} (see Supporting Information). Together with the observation that no nanometer sized fibrillar stuctures with preferred orientation are present (Figure 3a), these scattering curves can be attributed to a silica network formed outside the cell walls.

3.3. Microfibrillar and Elelantary-fibrillar Development During Calcination

A very useful method to extract details out of SAXS data is the inverse Fourier transformation method, leading to the so called pair distance distribution function.[34] Since the shape of the fibrillar structures in our data can be treated to be cylindrically symmetric, it is convenient to compute the cross section pair distance distribution function $p_c(r)$ from of the experimental scattering curves. The $p_c(r)$ function contains solely information on the fibril cross section in real space, i.e. their size, distribution and homogeneity. More information can be found in the supplementary information and in.[35,36] **Figure 5** shows the $p_c(r)$ functions for the delignified samples at different temperatures. The non-infiltrated delignified sample (*delig*) exhibits at low temperatures a single broad peak within $0 < r < 8$–10 nm, indicating largely equi-axed (e.g., circular) cross-section shape of the fibrils with homogeneous electron density distribution. The fibril diameters are, according to the minimum of the curve, approximately 12–14 nm. Heating leads to an increased destruction of all nanometer structures, demonstrated by the very broad peaks in the $p_c(r)$ function. In contrast, if the sample was infiltrated with TEOS, the $p_c(r)$ function from higher temperatures shows progressively stronger oscillations at small distances (Figure 5b), which is a clear indication of a non-homogeneous electron density distribution (i.e., substructures) within the fibrils. $p_c(r)$ has maxima at 0.8 nm and 3.5 nm and a minimum at about 2 nm. The peculiar shape of this curve is very similar to the real space curves observed for sub-particles at a high volume fraction.[36] We therefore conclude that the oscillations are the signature of rather densely packed parallel cylindrical sub-structures with diameters of about 2 nm. We note that albeit the high volume fraction, these cylinders are not perfectly ordered in a crystalline lattice, since this would give rise to a Bragg-peak in $I(q)$ and a peak in $p_c(r)$ at 3.5 nm that is higher than the one at 0.8 nm.[36]

The oscillations at small distances of the $p_c(r)$ function unambiguously demonstrate that not only the microfibrils but also the elementary fibrils have been replicated in the delignified and TEOS infiltrated samples after calcination. The MA sample series shows a behavior that is very similar (see Supporting Information). Hence, while the replication of the hierarchical levels down

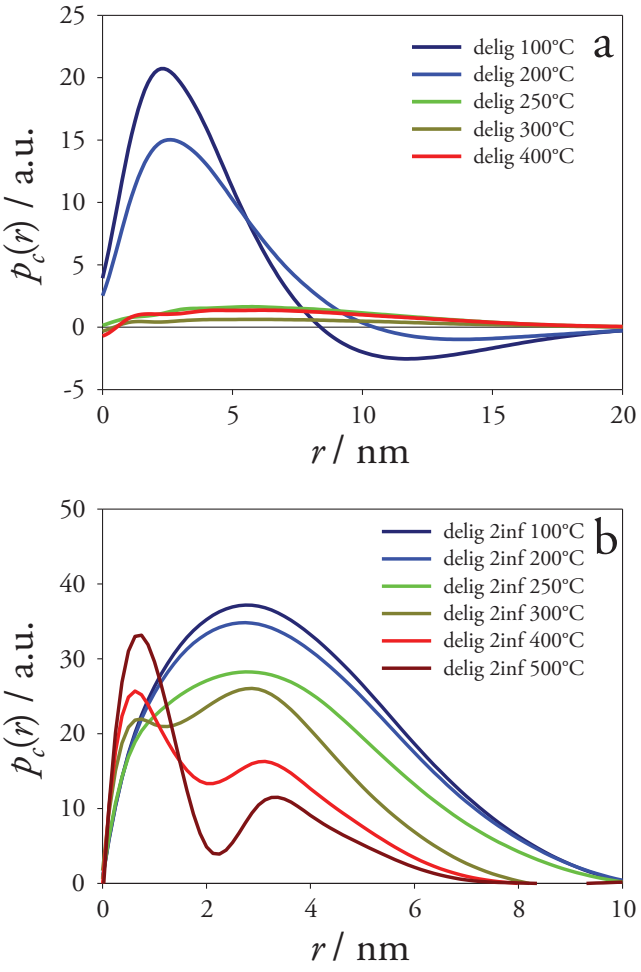

Figure 5. Temperature dependence of the cross section pair distance distribution function of delignified wood samples: a) without further treatment and b) after infiltration with TEOS.

to the microfibrillar level has previously been reported for this material,[31] the present finding shows that also the cellulose elementary fibril level can been replicated into cylindrical pores of ≈2 nm diameter in a silica matrix after calcination at 500 °C. The stability of the structures at higher temperatures was also investigated on a maleic acid anhydride functionalized sample (MA 2inf, see Supporting Information). Up to 625 °C no significant changes were observed. Higher temperatures, however, resulted in the loss of the inhomogeneous elementary fibril structure, i.e., the sub-structures of the microfibrils collapsed. At the same time, large, non-cylindrical structures occurred in the $p(r)$ functions (see Supporting Information), and also the degree of orientation started to diminish. Some elongated structures and a small degree of orientation were maintained up to 900 °C, where finally all nanostructural features were lost within 20 min.

3.4. Model Calculations

In order to describe the in situ calcination process quantitatively, a simple structural model based on the one proposed by

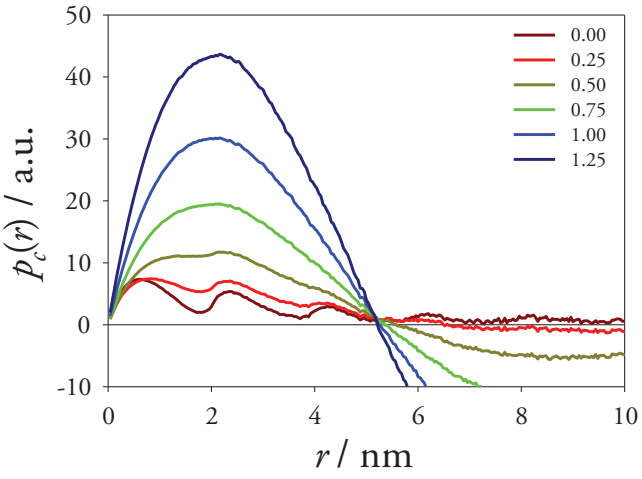

Figure 6. Cross section pair distance distribution functions of the model for different electron density ratios between microfibrils and impregnated hemicelluloses.

Fahlén and Salmén[13] was constructed (see Figure 1 and Section 6). Corresponding model calculations resulting in $p_c(r)$ functions are shown in **Figure 6**. They differ according to the ratio of the electron density of the elementary fibrils relative to that of the surrounding material in the microfibrils, the electron density ratio, **Table 1**. An electron density ratio of 1.25 leads to a curve in which hardly any oscillations are visible and which could easily be mistaken for a homogeneous cross section. This behavior is also found in the curves that were experimentally obtained from the delignified and the maleic acid anhydride functionalized sample series at low temperatures. Decreasing the electron density ratio below 0.5 leads to $p_c(r)$ functions, which show increasing oscillations at small distances, similar to the measurements from the samples delig 2inf, MA inf, and MA 2inf at high temperatures, Figure 6. This simple, semi-quantitative comparison leads to the conclusion that the electron density ratio of the elementary fibrils with respect to the surrounding material of the microfibrils is close to one at low temperatures and close to zero at high temperatures.

Differences between calculated and measured $p_c(r)$ curves are mostly visible at distances, where the detailed arrangement of the elementary fibrils within the microfibrils and the arrangement of the microfibrils themselves become important (i.e., at distances larger than 5–6 nm). They clearly reflect the crudeness of our model, which consists of monodisperse and circular elementary fibrils within circular microfibrils. Elliptical fibril cross sections would for instance lead to tails in the pair distance distribution functions, damping the oscillations at larger distances considerably.[35] This is the reason, why the higher orders of the oscillations are more pronounced in the calculated curves than in the experimental ones. These details can, however, be neglected at small distances corresponding approximately to the diameters of the elementary fibrils, which are dominated by the contrast between one individual elementary fibril and its surrounding medium. A least squares approximation of the experimentally obtained curves with the model curves within the range of distances from 0 nm to 2 nm therefore gives a reliable quantitative estimation of the electron density ratio of the elementary fibrils compared to the continuous phase of the microfibrils.

Table 1. Mass densities (ρ), electron densities (ρ_e), and electron density ratios of the materials used in the model. The densities of the hemicelluloses are estimates because their detailed structure and composition in the cell wall is not very well known. The electron density of hemicelluloses is estimated from the formula $C_{12}H_{22}O_{11}$.

	ρ [g/mL]	ρ_e [e^-/mL]	$\rho_e/\rho_{e,Hemicellulose}$
Cellulose	1.60 *[40]*	5.12×10^{23}	1.07
Hemicellulose	1.50 *[40]*	4.80×10^{23}	1.00
Silica	2.20 *[44]*	6.60×10^{23}	1.37

3.5. Development of the Electron Density Ratio

Figure 7 shows the development of the electron density ratio with temperature, obtained from the model approximation to the $p_c(r)$ functions for the delig and the MA samples, both

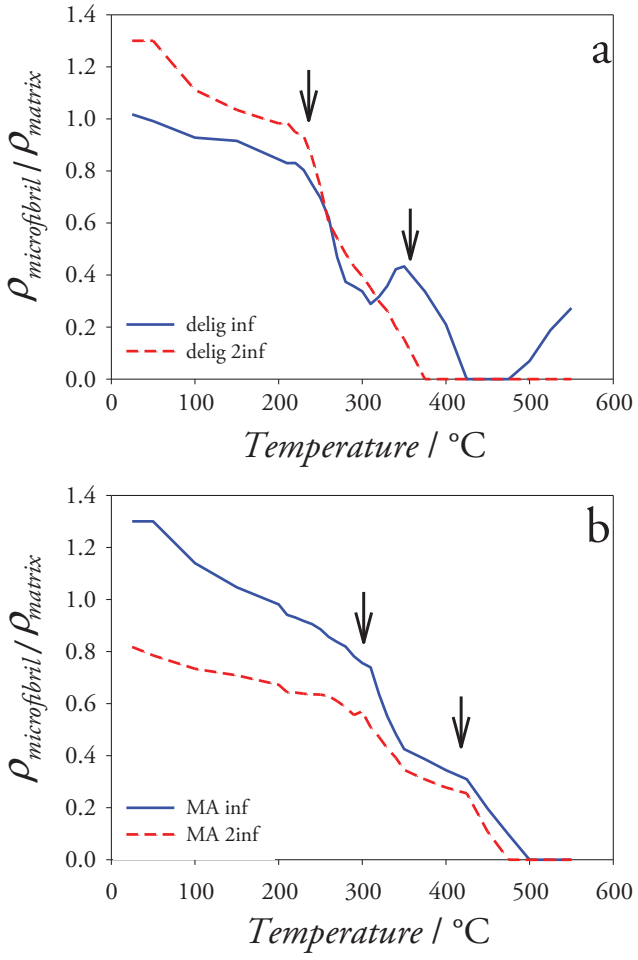

Figure 7. Temperature dependence of the electron density ratio between microfibrils and the hemicelluloses/silica material for a) delignified and b) maleic acid anhydride modified wood. The arrows indicate the onset of hemicelluloses and of cellulose disintegration (from Figure 8).

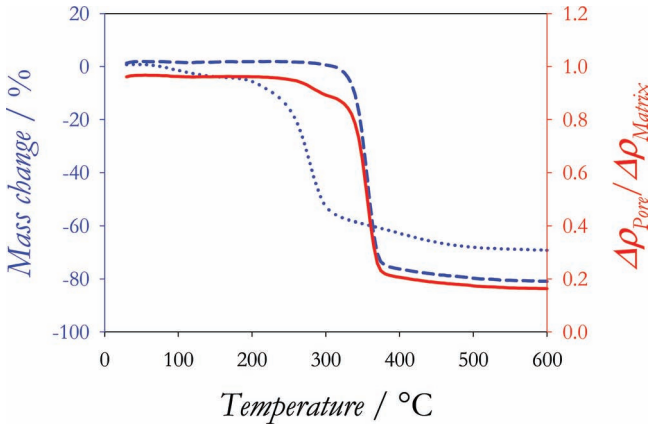

Figure 8. Thermogravimetric data for the pyrolysis of cellulose (dashed) and xylane (dotted). The solid line is the predicted electron density ratio from the thermogravimetric data.

infiltrated with TEOS. The ratio of the electron density of the elementary fibrils relative to that of the surrounding matrix phase decreases first slowly upon heating. This behavior turns into a sharp, step-like decrease starting at about 250 °C. At about 300 °C, a plateau at an electron density ratio of ≈0.4 is reached. A second, pronounced decrease of the electron density ratio to a value close to zero is observed between 350–430 °C. The behavior of the infiltrated maleic acid anhydride functionalized samples (Figure 7b) is very similar to the non-functionalized samples (Figure 7a). The two steps in electron density ratio are of similar height, but shifted to higher temperatures. This general behavior with two step-like changes of the electron density can be rationalized by the thermal behavior of the components of the nanocomposite material before calcination.

Thermogravimetric analysis of the pyrolysis of xylan (as a model for hemicelluloses) shows a strong decrease in mass at temperatures between 200–300 °C, while cellulose disintegrates at considerably higher temperatures of 300–380 °C (**Figure 8**). Comparing this with Figure 7 suggests the first step being due to the disintegration of hemicellulose, while the second step of the electron density ratio may be attributed to cellulose decomposition. We note however that the actual process during the in situ experiment was probably a mixture of both, pyrolysis and oxidation. Oxidation will depend on the actual accessibility of the structural elements for oxygen, with the combustion not necessarily taking place at the same temperature as the carbonization. The further discussion is based on the pyrolysis curves given in Figure 8 for two reasons: firstly in order to reduce the parameter space, and secondly because a thermogravimetry of wood samples in the presence of oxygen shows two steps very similar to the pyrolysis of the components.[31]

In order to assess the electron density ratio curves in Figure 7 in more detail, it is important to look more closely to the absolute numbers of the electron densities (Table 1). The final materials are porous silica, with the cell lumina and the original lignin parts within the cell walls being assumed to be empty with electron densities close to zero. One can assume that the initial electron density ratio at low temperatures is close to the ratio one would find for cellulose in a mixture of hemicelluloses and silica. Since the electron density of cellulose is larger than the one of hemicelluloses but smaller than the one of silica, the initial electron density ratio is expectedly close to one, as sketched in Figure 1b. Heating the samples first leads to the disintegration of the hemicelluloses. The cellulose elementary fibrils are then embedded in a silica matrix with the expected ratio of $\rho_{e,Cellulose}/\rho_{e,Silica} \approx 0.77$ after the first step. The second step in the electron density ratio curves corresponds to the disintegration of cellulose. After this step there should be empty pores within the silica, which corresponds to the electron density ratio of zero found in the experiments.

The changes in the electron density based on the scattering data can be compared to the mass loss curves obtained from thermogravimetric analyses (see Figure 8). A model curve for the electron density development of silicified wood based on the thermogravimetric data is drawn in Figure 8. This curve is based on the assumption that the microfibrils were originally embedded in a mixture of 33% silica and 67% hemicelluloses, which is based on the mass change due to infiltration found for twice infiltrated delignified sample delig 2inf.[31] Such a curve reproduces the experimentally observed two steps at 200–300 °C and at 300–400 °C, corresponding to the disintegration of hemicelluloses and of cellulose, respectively. A more quantitative comparison with the curves in Figure 7 is hampered by four factors. First, the experimental data are treated assuming that the microfibril angle was zero and only the S2 layer contributes to the scattering. This leads to inaccuracies in the experimental $p_c(r)$ functions. Second, the simple model taken to approximate the data is based on an idealized structure of the cell wall, which might lead to errors in the absolute values of the electron density ratio, while its trend should be correct. This is especially the case for the once delignified sample where the pair distance distribution function shows that non-cylindrical structures are also present (see Supporting Information). The third reason is caused by temperature shifts of the disintegration processes of the biopolymers. The modified and infiltrated organic compounds within the material might disintegrate at different temperatures than in their natural state. Additionally, the heating rate does also play a role. Slower heating can lead to disintegration of the substances at lower temperatures. This effect of the temperature protocol was verified with a MA 2inf. The holding time between the experiments was chosen five times longer and more temperature steps were measured. The behavior of the sample was similar to the one using the standard heating procedure. The height of the two steps did not change noticeable, although the steps themselves were shifted by almost 50 °C to lower temperatures. Finally the contribution of combustion relative to carbonization and their temperature dependence is not known for the various components within the sample.

4. Conclusions

The replication of the fibrillar wood structure into ceramics or silica has already been demonstrated in earlier work.[28–31] Here we have shown for the first time that delignified, optionally functionalized and TEOS infiltrated spruce wood transforms into silica replicas with a perfect replication also of the lowest hierarchical level, i.e., the level of the original crystalline cellulose

elementary fibrils upon calcination at 500 °C. This certainly opens new application potentials for these novel functional materials, since they contain helical nanopores of only about 2 nm diameter within the walls of a well preserved hierarchical porous system with macroscopically directional porosity.

The structural picture and its development with calcination temperature as sketched in Figure 1 could be deduced from in situ SAXS during calcination including extensive structure modeling. The results are supported and corroborated by TEM from entire cell wall sections of the calcined materials. It is proposed that the final structure is formed in two steps. At 250–300 °C, disintegration of the precursor infiltrated hemicelluloses takes place, leaving a stable silica network in the form of long fibrils of about 10 nm diameter with embedded, still at least partly intact cellulose microfibrils. At temperatures of about 350–450 °C the cellulose elementary fibrils also disintegrate, leaving corresponding nanopores of about 2 nm diameter within the silica fibrils. These structures are stable up to at least 625 °C, but fully destroyed at 900 °C.

5. Experimental Section

The sample preparation has been described in detail elsewhere.[31] In short, normal wood radial sections of 300 µm thickness were cut from the sapwood of spruce tree trunks (*Picea abies*). The microfibril angle of all samples was below 5°. The samples were first washed in a 2:1 mixture by weight of toluene and ethanol and then by ethanol using a Soxhlet apparatus (samples extr). Extracted samples were delignified in an aqueous solution of sodium chlorite and acetic acid (samples delig). Some of the delignified samples were modified further using a solution of maleic acid anhydride in dimethylacetamide, using triethylamine as a catalyst (samples MA).[37] Specimens of all three types of templates (extr, delig, and MA) were infiltrated with a solution of tetraethyl orthosilicate (TEOS) in ethanol. The samples were kept at 50 °C until the ethanol was evaporated and then dried at 85 °C and 110 °C (samples extr inf, delig inf, and MA inf). Some of these were subjected to a second cycle of TEOS infiltration (samples extr 2inf, delig 2inf, and MA 2inf).

Small-angle X-ray experiments were performed using the SAXS setup at the μ-spot beamline of the BESSY II storage ring at the Helmholtz Centre Berlin.[38] The wavelength used for the experiments was 0.10332 nm. In situ sample heating was performed with a custom made lamp furnace.[39] The samples were positioned between two copper plates that had a hole of 1.5 mm diameter. The plates were screwed to a thermocouple and the focus of a 150 W halogen lamp was directed onto the plates. The intensity of the halogen lamp was regulated by a temperature controller (Eurotherm 2000, Worthing, UK) in order to reach a predefined temperature. The samples were oriented with the tracheid direction perpendicular to the direction of the X-ray beam. The sample detector distance was 885 mm, of which 750 mm were through a He-filled tube with Kapton windows in order to reduce scattering by air. The scattering patterns were recorded using a phosphor screen coupled to a CCD detector (MarMosaic MX-225, Evanston, USA) with 3072 pixels × 3072 pixels of size 73 µm × 73 µm each.

The heating protocol was as follows: After setting the temperature to the desired value, the sample was kept for one minute prior to the actual X-ray exposure of 10 s. The temperature steps were: room temperature, 50 °C, 100 °C, 150 °C, and 200 °C. From 200°C to 350 °C, steps of 10 °C were used. From 350 °C to 550 °C the step size was increased to 25 °C. Finally, the sample was cooled down and measured again at room temperature. A high temperature series was measured for sample MA 2inf after the above mentioned protocol, comprising temperatures from 575 °C up to 900 °C in steps of 25 °C. The measurement at 900 °C was repeated 4 times with 10 min between the measurements to test for time dependent changes. For the same reason, sample MA 2inf was also measured using steps of 10 °C from 30 °C up to 550 °C with holding times of 5 min at each temperature prior to exposure.

The scattering pattern of the empty sample holder was subtracted from the transmission-corrected 2D scattering patterns of the samples. Then the patterns were multiplied with $\sin(\chi)$, where χ is the angle between a direction on the detector and the fiber direction of the wood. Scattering curves $I(q)$ were calculated from these patterns, where q is the absolute value of the scattering vector defined as $q = 4\pi/\lambda \sin(\theta/2)$, and λ and θ are the wavelength and the scattering angle, respectively. The multiplication with $\sin(\chi)$ makes the $I(q)$ identical to the curve one would obtain for a random orientation of the fiber directions provided that the fibers were originally close to parallel.[40] A second curve $I(\chi)$ was obtained by averaging all the pixels within one degree of χ and within the q-range from 1.14 nm^{-1} to 1.90 nm^{-1}.

The calculation of the orientation averaged scattering curves was based on the assumption that all the fibers within the scattering volume are parallel. Strictly speaking this cannot be the case in wood, since the cell walls P, S1, S2, and S3 all have a different orientation of the fibrils.[41] But due to the fact that the S2 layer dominates the cell wall volume, the other contributions were neglected. The helical arrangement of the fibrils around the cell also means that the fibrils at opposing sides of each wood cell are inclined at an angle to one another. This deviation from a parallel arrangement is small for normal wood, where the microfibril angle is 3°–5°. This simplification was justified by the observation that no splitting of the scattering pattern due to a high microfibril angle was observed in the azimuthally averaged scattering curves $I(\chi)$.[18]

Cross section pair distance distribution functions $p_c(r)$ can be calculated for cylinders, where the scattering curve can be separated into a length and a cross section term:

$$I(q) = \frac{\pi L}{q} 2\pi \int p_c(r) J_0(qr)\, dr \quad (1)$$

L is the length of the cylinders and J_0 is the zeroth order Bessel function. The $p_c(r)$ functions were obtained by means of indirect Fourier transformation.[42]

For transmission electron microscopy (TEM) imaging, samples were calcinated according to the heating protocol reported previously.[31] The samples were embedded into resin and cut to 80-nm-thick sections with an ultramicrotome. A TEM (CM30; Philips, Einhoven, The Netherlands) with an attached charge-coupled device camera (FastScan-F114; Tietz Video and Image Processing Systems, Gauting, Germany) was used for imaging at an acceleration voltage of 300 kV and under parallel illumination.

Thermogravimetric analysis (TGA) and differential thermal analysis (DTA) curves of all samples and pure cellulose (Sigma-Aldrich, Munich, Germany) and xylane (Adrich, Steinheim, Germany) were simultaneously recorded in air with a heating rate of 300 °C/h on a combined TGA/DTA device (STA 409, Netzsch Gerätebau, Selb, Germany).

6. Structural Model

The structural model (Figure 1) consisted of inhomogeneous parallel microfibrils (containing elementary fibrils with a different electron density) in a homogeneous surrounding medium. Since we assumed fiber symmetry, a 2D dimensional model was sufficient. Twelve circular fibrils were arranged in a two-dimensional box with a size of 1914 nm^2 in a way that they covered 70.9% of the area, which corresponds to the typical cellulose/hemicelluloses content within the S2 cell wall of spruce wood.[43] The diameters of the fibrils were polydisperse resulting in a normal distribution of the cross section areas with a mean area of 122 nm^2 and a standard deviation of 36 nm^2, corresponding to fibrils of 12.6 ± 6.8 nm in diameter. Circular microfibrils with a diameter of 2.67 nm were distributed within these fibrils covering 44.4% of the area of the box, which corresponds to 62.6% of the area of the fibrils. Again, these

values reflect the cellulose content in spruce wood.[43] Figure 1a shows a schematic representation of the model.

As the samples were delignified, we assumed that the medium surrounding the fibrils consists largely of porous space exhibiting zero electron density. A series of different electron density ratios between the continuous phase within the fibrils and the microfibrils was calculated. The ratios ranged from 0 to 1.3. This includes the estimated ratio of 1.07 between he electron densities of pure cellulose and hemicelluloses (see Table 1). The pair distance distribution function $p_c(r)$ was computed from these data using a Monte Carlo integration algorithm.[35] The various electron density ratios resulted in a set of $p_c(r)$ functions of the model.

The change of diameter of the experimental curves due to shrinkage was estimated from the shift of the position of the minimum in their $p_c(r)$ at r-values around 9–13 nm. The abscissae of the $p_c(r)$ curves from the model were scaled using this factor. The rescaled functions were approximated to the experimental data within the range of $0 < r < 2$ nm using a least squares approach and resulting in an estimation of the electron density ratio within the sample.

Supporting Information

Supporting Information is available from the Wiley Online Library or from the author.

Acknowledgements

The authors thank Chenghao Li and Stefan Siegel for supporting the synchrotron experiments. Funding of the project "Hierarchically structured porous ceramics and composites from nanocasting of plant cell wall" in the framework of the priority programme SPP1420 by the German Research Foundation (Deutsche Forschungsgesellschaft) is gratefully acknowledged.

Received: June 20, 2012
Revised: August 31, 2012
Published online: October 12, 2012

[1] S. Mann, *Biomineralization: Principles and Concepts in Bioinorganic Materials Chemistry*, Oxford University Press, Oxford **2001**.
[2] T.-X. Fan, S.-K. Chow, D. Zhang, *Prog. Mater. Sci.* **2009**, *54*, 542.
[3] J. Will, C. Zollfrank, A. Kaindl, H. Sieber, P. Greil, *Keram. Z.* **2010**, *62*, 114.
[4] B. Bhushan, *Philos. Trans. R. Soc.* **2009**, *A 367*, 1445.
[5] A. Zampieri, W. Schweiger, C. Zollfrank, P. Greil, in *Handbook of Biomineralization*, (Ed: E. Baeuerlein), Wiley-VCH, Weinheim **2007**.
[6] S. Zhu, D. Zhang, Z. Li, H. Furukawa, Z. Chen, *Langmuir* **2008**, *24*, 6292.
[7] C. Zollfrank, P. Cromme, M. W. Rauch, H. Scheel, M. H. Kostova, K. Gutbrod, S. Gruber, D. Van Opdenbosch, *Bioinspired, Biomimetic Nanobiomater.* **2012**, *1*, 13.
[8] O. Paris, I. Burgert, P. Fratzl, *MRS Bull.* **2010**, *35*, 219.
[9] H. O. Fabritius, C. Sachs, P. R. Triguero, D. Raabe, *Adv. Mater.* **2009**, *21*, 391.
[10] A. Al-Sawalmih, C. Li, S. Siegel, P. Fratzl, O. Paris, *Adv. Mater.* **2009**, *21*, 4011.
[11] L. Sapei, R. Noeske, P. Strauch, O. Paris, *Chem. Mater.* **2008**, *20*, 2020.
[12] D. Fengel, G. Wegener, *Wood: Chemistry, Ultrastructure, Reactions*, Walter de Gruyter, Berlin, New York **1984**.
[13] J. Fahlén, L. Salmén, *Biomacromolecules* **2005**, *6*, 433.
[14] D. Fengel, *TAPPI* **1970**, *53*, 497.
[15] A. Kerr, D. Goring, *Cellul. Chem. Technol.* **1975**, *9*, 563.
[16] J. Sell, T. Zimmermann, *Holz Roh-Werkst.* **1993**, *51*, 384.
[17] D. Fengel, M. Stoll, *Holzforschung* **1973**, *27*, 1.
[18] H. Lichtenegger, A. Reiterer, S. E. Stanzl-Tschegg, P. Fratzl, *J. Struct. Biol.* **1999**, *128*, 257.
[19] H. F. Jakob, D. Fengel, S. E. Tschegg, P. Fratzl, *Macromolecules* **1995**, *28*, 8782.
[20] R. W. Drum, *Science* **1968**, *161*, 175.
[21] C. E. Byrne, D. C. Nagle, *Carbon* **1997**, *35*, 259.
[22] P. Greil, *J. Eur. Ceram. Soc.* **2001**, *21*, 105.
[23] C. Zollfrank, H. Sieber, *J. Eur. Ceram. Soc.* **2004**, *24*, 495.
[24] J. Cao, C. R. Rambo, H. Sieber, *J. Porous Mater.* **2004**, *11*, 163.
[25] O. Paris, C. Zollfrank, G. A. Zickler, *Carbon* **2005**, *43*, 53.
[26] C. Zollfrank, J. Fromm, *Holzforschung* **2009**, *63*, 248.
[27] D. Van Opdenbosch, M. H. Kostova, S. Gruber, S. Krolikowski, P. Greil, C. Zollfrank, *Wood Sci. Technol.* **2010**, *44*, 547.
[28] Y. Shin, J. Liu, J. H. Chang, Z. Nie, G. J. Exarhos, *Adv. Mater.* **2001**, *13*, 728.
[29] P. V. Persson, J. Hadrén, A. Fogden, G. Daniel, T. Iversen, *Biomacromolecules* **2004**, *4*, 1097.
[30] A. S. Deshpande, I. Burgert, O. Paris, *Small* **2006**, *2*, 994.
[31] D. Van Opdenbosch, G. Fritz-Popovski, O. Paris, C. Zollfrank, *J. Mater. Res.* **2011**, *26*, 1193.
[32] S. L. LeVan, in *Concise Encyclopedia of Wood & Wood Based Materials*, (Ed: A. P. Schniewind), Pergamon Press, Elmsford **1989**, 271.
[33] G. Porod, *Kolloid-Z.* **1951**, *124*, 83.
[34] O. Glatter, in *Small Angle X-ray Scattering*, (Eds: O. Glatter, C. Kratky), Academic Press, London **1982**.
[35] G. Fritz, A. Bergmann, *J. Appl. Cryst.* **2004**, *37*, 815.
[36] G. Fritz-Popovski, A. Bergmann, O. Glatter, *Phys. Chem. Chem. Phys.* **2011**, *13*, 5872.
[37] C. Zollfrank, R. Kladny, H. Sieber, P. Greil, *J. Eur. Ceram. Soc.* **2004**, *24*, 479.
[38] O. Paris, L. Chenghao, S. Siegel, G. Weseloh, F. Emmerling, H. Riesmeier, A. Erko, P. Fratzl, *J. Appl. Crystallogr.* **2007**, *40*, s466.
[39] G. A. Zickler, W. Wagermaier, S. S. Funari, M. Bughammer, O. Paris, *J. Anal. Appl. Pyrolysis* **2007**, *80*, 134.
[40] H. F. Jakob, S. E. Tschegg, P. Fratzl, *Macromolecules* **1996**, *29*, 8435.
[41] J. R. Barnett, V. A. Bonham, *Biol. Rev.* **2004**, *79*, 461.
[42] O. Glatter, *J. Appl. Crystallogr.* **1980**, *13*, 577.
[43] E. Sjöström, *Wood Chemistry, fundamentals and applications*, Vol. *2*, Academic Press, New York **1993**.
[44] N. N. Greenwood, A. Earnshaw, *Chemistry of the Elements*, Pergamon Press, Oxford **1984**.